PCCP

Accepted Manuscript

ROYAL SOCIETY OF CHEMISTRY

www.rsc.org/pccp

Physical Chemistry Chemical Physics

ARTICLE

Effect of Cation Substitution on Structural Transition: Synthesis, Characterization and Theoretical Studies of $NaCa_4B_3O_9$, $NaCaBO_3$, $NaSrBO_3$ and $Li_4CaB_2O_6$

Received 00th January 20xx,
Accepted 00th January 20xx

DOI: 10.1039/x0xx00000x

www.rsc.org/

Yun Yang,[a] Xin Su,[a,b] Shilie Pan,*[a] and Zhihua Yang[a]

Single crystals of $NaCa_4B_3O_9$, $NaCaBO_3$, $NaSrBO_3$ and $Li_4CaB_2O_6$ have been successfully synthesized through conventional high-temperature solid-state reactions. They are structurally characterized by single crystal X-ray diffraction and exhibit three-dimensional crystal structures consisting of isolated planar BO_3 as fundamental building blocks. Interestingly, for the centrosymmetric crystal structure $NaCaBO_3$ ($Na_3Ca_3B_3O_9$), as 2/3 Na^+ ions are substituted by Ca^{2+} ions, $NaCa_4B_3O_9$ is obtained and crystallizes in a noncentrosymmetric space group *Ama*2 (crystal class *mm*2). Second harmonic generation (SHG) test of the title compound by the Kurtz–Perry method shows that $NaCa_4B_3O_9$ can be phase matchable with an effective SHG coefficient approximately about one-half times that of KH_2PO_4 (KDP). Studies of their optical properties as well as band structure calculations based on density functional theory methods have been also performed. $NaCa_4B_3O_9$ possesses a moderate birefringence about 0.05 at 1064 nm. To explain the difference in optical nonlinearity we compared the electronic structures of $NaCa_4B_3O_9$, $KCa_4B_3O_9$ and $KSr_4B_3O_9$ crystals, in particular at the bottom of conduction band (CB) and the top of valence band (VB), since they are known to play a primary role in SHG. These electronic structures are responsible for the optical-nonlinearity of $NaCa_4B_3O_9$, $KCa_4B_3O_9$ and $KSr_4B_3O_9$ crystals.

1. Introduction

Studies of polar materials have attracted great interest due to their technologically important properties: pyroelectricity and ferroelectricity, *etc*.[1,2] To synthesize materials with desired physical or chemical properties, chemical reactions are often planned on controlling the topology of inorganic frameworks. Generally, for a solid-state material to be considered polar, the compound must crystallize in one of ten crystal classes: 1, 2, 3, 4, 6, *m*, *mm*2, 3*m*, 4*mm*, or 6*mm*.[1] Clearly, polarity and polar materials are important, yet the question of how to synthesize a new polar material remains. It is found that the size, shape and charge of the template cations may direct the formation of different open frameworks.[2-10] For example, two new borate halides, $NaBa_4(AlB_4O_9)_2Br_3$ and $NaBa_4(B_5O_9)_2F_2Cl$, have similar stoichiometry, they exhibit obviously different structures. $NaBa_4(AlB_4O_9)_2Br_3$ is noncentrosymmetric (NCS) and polar, while $NaBa_4(B_5O_9)_2F_2Cl$ is centrosymmetric (CS). It shows that the difference is mainly due to the rigid AlO_4 tetrahedra reducing the degree of freedom of the connection of the building units and increasing the distortion of B−O groups in the framework.[7a] For the series of stoichiometric crystals $K_{3-x}Na_xB_6O_{10}Br$ (x = 0.13, 0.67, 1.30, 2.20), interestingly, the Na^+ concentration plays a profound role to influence the crystal structure. Up to about 23% (x = 0.7) the K^+ ions can be substituted by the Na^+ ions with the same NCS crystal structure of $K_3B_6O_{10}Br$ (space group *R*3*m*) being retained, while a higher Na concentration would lead to it crystallize in the CS space group *Pnma*. The different Br-M (M = K/Na, K, or Na) lattices, which are influenced by the coordination environments of the cations, are responsible for the structural changes from NCS to CS.[7b]

One goal of this research is to get insight into the structure-property relationships and to promote novel synthetic routes to new NLO materials with interesting properties. The combination of alkali- or alkaline-earth metal with borate system[7,11] is one approach that can be used to design new NLO materials with excellent performance, such as β-BaB_2O_4 (BBO),[12a] LiB_3O_5 (LBO),[13a] CsB_3O_5 (CBO),[14a] $CsLiB_6O_{10}$ (CLBO)[15a], $KBe_2BO_3F_2$ (KBBF)[16a], $Na_2Be_4B_4O_{11}$[5a], $LiNa_5Be_{12}B_{12}O_{33}$[5a], and so on. The practical potential of those materials is mostly associated with the structure characteristics of the boron-oxygen groups.[11-24]

To date, about a dozen borates have been synthesized and structurally determined, and of these, only several crystals are polar. For X. L. Chen's group, in searching new optical materials with $[BO_3]^{3-}$ anionic groups, a serial mixed alkali- or alkaline-earth borate compound have been well determined by the SDPD (structure determination from powder diffraction) method systems.[25] And the series noncentrosymmetric borates, $MM'_4(BO_3)_3$ (M = Na, M′ = Ca; M = K, M′ = Ca, Sr) which crystallize in the polar space group

[a] *Key Laboratory of Functional Materials and Devices for Special Environments, Xinjiang Technical Institute of Physics & Chemistry, Chinese Academy of Sciences; Xinjiang Key Laboratory of Electronic Information Materials and Devices, 40-1 South Beijing Road, Urumqi 830011, China.*
[b] *University of Chinese Academy of Sciences, Beijing 100049, China.*
Electronic Supplementary Information (ESI) available: [crystal data (CIF files), interatomic distances and angles, bond valences, figures of powder X-ray diffraction, crystal structures and calculated band structures]. See DOI: 10.1039/x0xx00000x

*Ama*2 arouse our interest. In our group, a continuous effort in the alkali- or alkaline-earth borate system has led to four compounds $NaCa_4B_3O_9$, $NaCaBO_3$, $NaSrBO_3$ and $Li_4CaB_2O_6$. Here these crystal structures were reinvestigated using the single-crystal X-ray diffraction. Through comparison and analysis, there are some interesting connections on structural transition. For the CS crystal structure $NaCaBO_3$ ($Na_3Ca_3B_3O_9$), as 2/3 Na^+ ions are substituted by the Ca^{2+} ions, $NaCa_4B_3O_9$ is obtained and crystallizes in a NCS space group *Ama*2. For another, $NaCaBO_3$ and $NaSrBO_3$ have a very similar chemical formula, but have different space groups. We wonder whether and how this substitution has the impact on the crystal structure and NLO properties.

Further understanding of the relationship between the structure and the properties of these compounds prompts us to carry out theoretical calculation. Theoretical exploration has suggested that anionic groups and chemical bonding structures have an important influence on the NLO properties of crystals.[22,23] The theoretical investigation of the band structure may play a crucial role in understanding of the physical properties and give predictions of the NLO susceptibilities. In this work, we present the synthesis, crystal growth, structure, calculation, and optical properties of them. And the influence of the cations substitution on structure and SHG property is discussed. A detailed depiction of the electronic and spectral features would bring us important insights in understanding the origin of the electronic band structure and densities of states. In addition, in this article we present a study on the mechanism of linear and NLO optical effects in $NaCa_4B_3O_9$, $KCa_4B_3O_9$ and $KSr_4B_3O_9$ crystals based on the generalized gradient approximation with DFT.[26] Up to now in the literature, there has been no systematic theoretical calculation combination experiments study on the linear and nonlinear optical properties of $NaCa_4B_3O_9$, $KCa_4B_3O_9$ and $KSr_4B_3O_9$ crystals. The refractive indices and birefringence of the above-mentioned crystals were calculated from their band structures. Finally, several useful results are given. This information is essential to the design and search for new NLO crystals.

2. Experimental Section

Crystal Growth and Compound Synthesis

Crystal Growth. Single crystals of $NaCa_4B_3O_9$ were grown by spontaneous crystallization using Na_2O−PbO−B_2O_3 as the flux system. A mixture of Na_2CO_3, $CaCl_2$, H_3BO_3 and PbO with a molar ratio of 7:4:10:2 melt in a platinum crucible, which was placed in the centre of a programmable temperature electric furnace. The furnace was gradually heated to 900 °C, held at this temperature for 20 h until the solution became transparent and clear. During the process of cooling, a platinum wire was intermittently dipped into the solution to try the initial crystallization temperature. When the temperature was cooled to 750 °C, there were some small crystals generated on the surface of solution. It then was further cooled to 550 °C at a rate of 2 °C/h, and then the temperature was allowed to cool to room temperature at a rate of 10 °C/h.

Similarly, single crystals of $NaCaBO_3$ were grown from a high temperature solution by using Na_2O−PbO−B_2O_3 as the flux system. The solution was prepared in a platinum crucible by melting a mixture of Na_2CO_3, $CaCl_2$, H_3BO_3 and PbO at a molar ratio of 4:1:3:1. The mixture was heated in a programmable temperature electric furnace at 850 °C and held at this temperature for 20 h. The homogenized solution was then cooled rapidly. When the temperature was cooled to 650 °C, there were some small crystals generated on the surface of solution. It then was further cooled to 500 °C at a rate of 2 °C/h. Finally, it was allowed to cool to room temperature at a rate of 10 °C/h.

Single crystals of $NaSrBO_3$ and $Li_4CaB_2O_6$ were grown from the high temperature solution using Na_2O−B_2O_3 and Li_2O−B_2O_3 as the flux systems, respectively. The solutions were prepared in a Pt crucible by melting a mixture of $NaNO_3$, $Sr(NO_3)_2$ and H_3BO_3 at a molar ratio of 6:2:5 for $NaSrBO_3$, as well as Li_2CO_3, $CaCO_3$ and H_3BO_3 at a molar ratio of 3:1:3 for $Li_4CaB_2O_6$. And then the Pt crucible was placed in the center of a programmable temperature furnace, gradually heated to 850 °C (800 °C), held at this temperature for 20 h, and then quickly cooled to the initial crystallization temperature 780 °C (720 °C) for $NaSrBO_3$ ($Li_4CaB_2O_6$). It then was further cooled to 500 °C at a rate of 2 °C/h. Finally, it was allowed to cool to room temperature.

Some colorless, transparent block crystals were obtained for structure determination.

Compound Synthesis. The polycrystalline powders of $NaCa_4B_3O_9$, $NaCaBO_3$, $NaSrBO_3$ and $Li_4CaB_2O_6$ were synthesized by traditional solid-state reaction techniques. The mixtures of Na_2CO_3, $CaCO_3$ and H_3BO_3 at a molar ratio 3:1:3 for $NaCa_4B_3O_9$; Na_2CO_3, $CaCO_3$/$SrCO_3$ and H_3BO_3 at a molar ratio 1:2:2 for $NaCaBO_3$ and $NaSrBO_3$; and Li_2CO_3, $CaCO_3$ and H_3BO_3 at a molar ratio 2:1:2 for $Li_4CaB_2O_6$ were ground well and packed into Pt crucibles, respectively. The raw materials were heated to 500 °C, and held for 10 h to decompose the carbonate and eliminate the water. They were then heated to 870 °C for $NaCa_4B_3O_9$, 750 °C for $NaCaBO_3$, 750 °C for $NaSrBO_3$ and 710 °C for $Li_4CaB_2O_6$ held for 48 h. The mixtures were ground between all heating. The powders of these compounds were obtained. The powder X-ray diffraction data were carried out with a Bruker D2 PHASER diffractometer equipped with a diffracted beam monochromator set for Cu Kα radiation (λ = 1.5418 Å). The diffraction patterns were taken from 10° to 70° (2θ) with a scan step width of 0.02° and a fixed counting time of 1 s/step. The diffraction patterns are agreeable with the calculated ones (Fig. S1, ESI†).

Characterization Techniques

X-ray Crystallographic Studies. A few millimetre-sized block crystals of $NaCa_4B_3O_9$, $NaCaBO_3$, $NaSrBO_3$ and $Li_4CaB_2O_6$ have been obtained by the above spontaneous crystallization technique for the structure determination. The single crystals of $NaCa_4B_3O_9$, $NaCaBO_3$, $NaSrBO_3$ and $Li_4CaB_2O_6$ with dimension 0.25 mm × 0.13 mm × 0.07 mm, 0.194 mm × 0.132 mm × 0.09 mm, 0.18 × 0.15 × 0.10 and 0.15 mm × 0.14 mm × 0.09 mm were selected for the structure determination, respectively. Their crystal structures were determined by single-crystal X-ray diffraction on an APEX II CCD diffractometer using monochromatic Mo Kα radiation (λ = 0.71073 Å) at 296(2) K and integrated with the SAINT program.[27] Numerical absorption corrections were carried out using the SCALE program for area detector.[27] All calculations were performed with programs from the SHELXTL crystallographic software package.[28] The structure was solved by direct methods using SHELXS-97.[29] All atoms were refined using full matrix least-squares techniques; Final least-squares refinement is on F_o^2 with data having $F_o^2 \geq 2\sigma(F_o^2)$. The structure was checked for missing symmetry elements with PLATON.[30] Crystal data and structure refinement information are

presented in Table 1. The final refined atomic positions and isotropic thermal parameters are listed in Table S1, ESI†. Selected bond distances (Å) and angles (°) for the four crystals are given in Table S2, ESI†.

UV-VIS-NIR Diffuse-Reflectance Spectroscopy. UV-VIS-NIR diffuse–reflectance of these compounds was collected with a SolidSpec-3700DUV spectrophotometer using fluororesin as a standard in the wavelength range from 190 to 2600 nm.

NLO Measurements. Powder SHG tests were carried out on $NaCa_4B_3O_9$ by the Kurtz–Perry method using 1064 nm radiation.[31] A detailed description of the equipment and the methodology used has been published.[32]

Numerical Calculation Details. The electronic structures calculations were performed using a plane-wave basis set and pseudopotentials within density functional theory (DFT) implemented in the total-energy module CASTEP.[33] The exchange and correlation effects were treated by Perdew–Burke–Ernzerhof (PBE) in the generalized gradient approximation (GGA).[26] The interactions between the ionic cores and the electrons were described by Norm-conserving pseudopotentials. The following orbital electrons were treated as valence electrons: Na $2s^2 2p^6 3s^1$, Li $1s^2 2s^1$, K $3s^2 3p^6 4s^1$, Sr $4s^2 4p^6 5s^2$, B $2s^2 2p^1$, O $2s^2 2p^4$, and Ca $3s^2 3p^6 4s^2$. The number of plane waves included in the basis was determined by a cutoff energy of 830 eV, and the numerical integration of the Brillouin zone was performed using a 4 × 4 × 3 Monkhorst–Pack scheme[34] k-point grid sampling for $NaCaBO_3$ and $NaCa_4B_3O_9$. The number of plane waves included in the basis was determined by a cutoff energy of 340 eV, and the numerical integration of the Brillouin zone was performed using a 3 × 3 × 2 Monkhorst–Pack scheme[34] k-point grid sampling for $KCa_4B_3O_9$ and $KSr_4B_3O_9$. Our test showed that these computational parameters ensure good convergence in the present studies. The linear optical response properties of the BHS crystal was examined through calculating the complex dielectric function $\varepsilon(\omega) = \varepsilon_1(\omega) + i\varepsilon_2(\omega)$. The imaginary part of the dielectric function ε_2 is given in the following equation:[35]

$$\varepsilon_2\left(q \to O_u, h\omega\right) = \frac{2e^2\pi}{\Omega\varepsilon_o}\sum_{kcv}\left|\left\langle\varphi_k^c\left|u\cdot r\right|\varphi_k^v\right\rangle\right|^2\delta\left[E_k^c - E_k^v - E\right]$$

The real part $\varepsilon_1(\omega)$ can be obtained from the imaginary part $\varepsilon_2(\omega)$ by the Kramers–Kronig transformation. All the other optical constants, such as the absorption spectrum, refractive index, and reflectivity are derived from $\varepsilon_1(\omega)$ and $\varepsilon_2(\omega)$.[36] The SHG coefficients are calculated from the band wave functions by using the so-called length-gauge formalism derived by Aversa and Sipe[37] at a zero frequency limit. The static second-order nonlinear susceptibilities $\chi\alpha\beta\gamma(2)$ can be reduced as,[38]

$$\chi_{\alpha\beta\gamma}^{(2)} = \chi_{\alpha\beta\gamma}^{(2)}(\mathrm{VE}) + \chi_{\alpha\beta\gamma}^{(2)}(\mathrm{VH}) + \chi_{\alpha\beta\gamma}^{(2)}(\text{two-bands})$$

In this sum-over-states type formalism, the total SHG coefficient $\chi(2)$ are divided into contribution from Virtual-Hole (VH), Virtual-Electron (VE) processes, and two-Band (TB) has been proved to be exactly zero.[39] Furthermore, the theoretical methods have also been applied with success to analyze the linear refractive indices and SHG coefficients of other NLO crystals, in our previous study.[39]

3. Results and Discussion

Crystal Structure

$NaCa_4B_3O_9$ crystallizes in space group *Ama*2 of the orthorhombic system. In the asymmetric unit, there are three unique Ca atoms, one unique Na atom, three unique B atoms, and six unique O atoms (Table S1, ESI†). Its average structure features a 3D network composed of NaO_8, CaO_n (n = 8, 9) distorted polyhedra, and isolated BO_3 units (Fig. S2, ESI†). The basic building units are isolated BO_3 groups (Fig. 1a). The B-O bond lengths range from 1.360(6) to 1.400(3) Å with an average value of 1.376 Å, and O-B-O bond angles are between 115.9(4) and 121.97(18)° (Table S2, ESI†), which is corresponding to the sp^2 hybridization of B atoms. Viewed along the *c*-axis, the $B(1)O_3$ and $B(2)O_3$ triangles are parallel with the (0 1 0) face and opposite to each other. All of the $B(3)O_3$ triangles have the same direction along the *c*-axis.

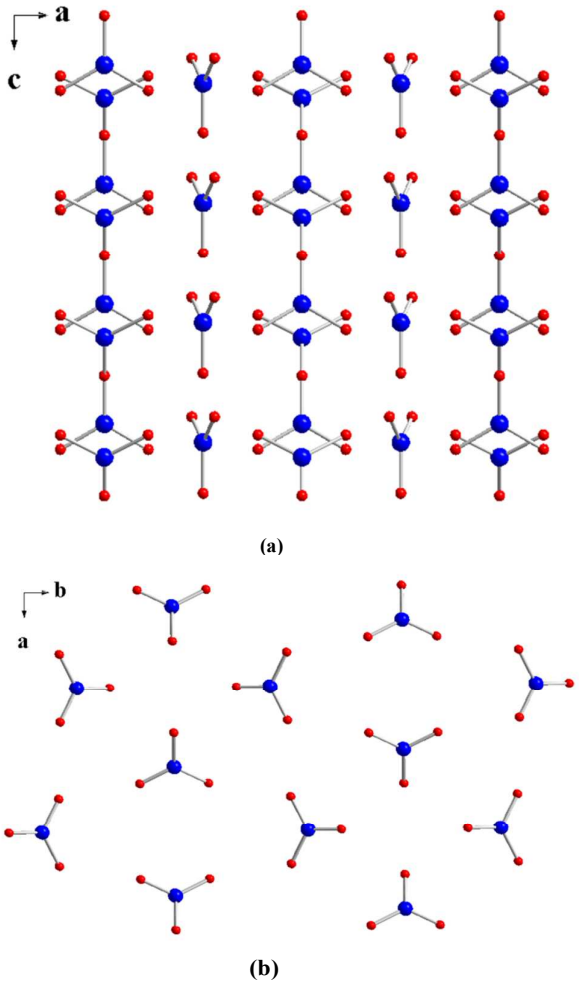

Fig. 1 Representation of isolated BO_3 structural building unit in (a) $NaCa_4B_3O_9$ and (b) $NaCaBO_3$.

The Na atom is eight-coordinated by eight O atoms in a distorted geometry with Na-O distances in the range 2.491(4)–2.992(3) Å. Every two neighboring 8–coordinated Na(1) atoms

Table 1. Crystal data and structure refinement for $NaCa_4B_3O_9$, $NaCaBO_3$, $NaSrBO_3$ and $Li_4CaB_2O_6$.

Empirical formula	$NaCa_4B_3O_9$	$NaCaBO_3$	$NaSrBO_3$	$Li_4CaB_2O_6$
Formula weight	359.74	121.88	169.42	185.46
Crystal system	Orthorhombic	Orthorhombic	Monoclinic	Orthorhombic
Space group	*Ama*2	*Pmmn*	$P2_1/c$	*Pnnm*
a (Å)	10.686(2)	10.190(2)	5.325(4)	9.277(12)
b (Å)	11.264(3)	16.078(4)	9.268(7)	8.100(10)
c (Å)	6.4834(13)	3.4894(8)	6.075(5)	3.488(5)
V (Å3)	780.4(3)	571.7(2)	294.6(4)	262.1(6)
Z	4	8	4	2
ρ(calcd) (g/cm^3)	3.062	2.832	3.819	2.350
μ (mm^{-1})	2.864	2.113	18.219	1.150
F(000)	712	480	312	180
θ (deg)	3.63 to 27.53	2.37 to 27.46	4.06 to 27.43	3.34 to 27.43
Limiting indices	-11≤ h≤13, -12≤k≤14, -8≤l≤8	-13≤h≤13,-15≤k≤20, -4≤l≤3	-6≤h≤6, -10≤k≤12, -6≤l≤7	-12≤k≤11, -10≤h≤8, -4≤3≤l
Reflections collected / unique	2097 / 920 [R(int) = 0.0243]	3273 / 719 [R(int) = 0.0280]	1744 / 669 [R(int) = 0.0260]	1594 / 350 [R(int) = 0.0245]
Completeness to theta	98.5 %	100.0 %	99.7 %	99.7 %
Data/restraints/parameters	920 / 1 / 89	719 / 0 / 67	669 / 0 / 55	350 / 0 / 42
Goodness-of-fit on F^2	1.063	1.171	1.088	1.264
Final R indices [F_o^2>2s(F_o^2)][a]	R1 = 0.0197, wR2 = 0.0490	R1 = 0.0212, wR2 = 0.0552	R1 = 0.0266, wR2 = 0.0541	R1 = 0.0209, wR2 = 0.0523
R indices (all data)[a]	R1 = 0.0204, wR2 = 0.0493	R1 = 0.0237, wR2 = 0.0574	R1 = 0.0329, wR2 = 0.0646	R1 = 0.0239, wR2 = 0.0661
Extinction coefficient	0.0108(8)	0.063(3)	0.0000(15)	0.23(2)
Largest diff. peak and hole (e•Å^{-3})	0.265 and -0.336	0.423 and -0.248	1.571 and -0.831 e	0.225 and -0.343
Flack parameter	0.11(5)	N/A	N/A	N/A

[a] $R_1 = \Sigma||F_o| - |F_c||/\Sigma|F_o|$ and $wR_2 = [\Sigma w(F_o^2 - F_c^2)^2/ \Sigma wF_o^4]^{1/2}$ for $F_o^2 > 2\sigma(F_o^2)$.

share bridging O(4) atoms into infinite 1D chains along *c* axis (Fig. S2b, ESI†). And a 3D framework are formed by bridging the B(2) atoms with 1D Na–O chains (Fig. S2c, ESI†). The $Ca(1)O_8$, $Ca(2)O_9$ and $Ca(3)O_8$ polyhedra are interconnected by shared oxygen atoms to form the 3D framework (see Fig. S2d, ESI†) with Ca–O bond distances ranging from 2.345(3) to 2.8772(15) Å. The isolated BO_3 units, Ca–O, Na–O groups connect with each other to form the whole 3D framework, in which each BO_3 unit is linked to four $Ca(1)O_8$, two $Ca(2)O_9$, two $Ca(3)O_8$ and two $Na(1)O_8$ polyhedra through sharing oxygen atoms.

Crystallographic analysis reveals that the $NaCaBO_3$ crystal belongs to the space group *Pmmn* of the orthorhombic system. Its structure exhibits a complicated 3D network composed of NaO_n (n=6, 8), CaO_6, Na/CaO_7 distorted polyhedra and isolated BO_3 groups that are interconnected via corner or edge sharing as shown in Fig. S3, ESI†. There are three unique Na atoms, two unique Ca atoms, two unique B atoms, and four unique O atoms (Table S1, ESI†). As illustrated in Fig. 2 and Fig. S3a, ESI†, the fundamental building units of $NaCaBO_3$ are isolated BO_3 groups. The B–O bond lengths vary from 1.368(3) to 1.382(3) Å with an average value of 1.376 Å, and the O-B-O angles are between 117.5(3) and 124.51(9)º (Table S2, ESI†). These values are normal in a BO_3 triangle. Ca(1) is surrounded by six O atoms to form a $Ca(1)O_6$ distorted octahedral geometry, in which the Ca(1)–O bond distances range from 2.2266(17) to 2.3915(18) Å. The $Ca(1)O_6$ polyhedra are interconnected via sharing edges into a 1D double chain along the *c* axis (Fig. S3b, ESI†). For Ca(2) and Na(1), the Ca^{2+} and Na^+ cations share the same sites with a mixed occupancy model of 75% Ca^{2+}/25% Na^+, the overall model refines very good (Fig. S3c, ESI†). The Ca(2)/Na(1) atom is surrounded by seven oxygen atoms forming a distorted polyhedral arrangement with Ca(2)/Na(1) bond lengths ranging from 2.3618(9)–2.6010(9) Å (*av* = 2.466 Å). The Ca(2)/Na(1) polyhedra are interconnected via sharing O(5) atom and edges into a 3D framework along the *c* axis (Fig. S3c, ESI†). Na(2) is strongly bonded to four O atoms at distances of 2.450 Å and also weakly bonded to four more O atoms at distances of 3.028 Å. Taking all these eight bonds into account, the concept of bond valence[10,40] allows us to calculate a valence sum equal to 0.835 for Na(2) which proves that the long bonds indeed participate in the metal coordination scheme (Table S3, ESI†). The eightfold coordination around Na(2) can be described as a highly distorted square prism. Each Na(3) atom is coordinated to six O atoms giving rise to a distorted trigonal prismatic arrangement. A parallel tunnel is formed by Na(2) and Na(3) atoms sharing O(3) atoms (Fig. S3d, ESI†).

$NaSrBO_3$ crystallizes in a monoclinic crystal system with a space group of $P2_1/c$. Because the radius of Sr atom is larger than the radius of the Ca atom, so when Ca^{2+} in the structure of $NaCaBO_3$ is substituted by Sr^{2+}, the symmetry of the original symmetry is reduced. As a result, the structure space group was translated from *Pmmn* to $P2_1/c$. In the asymmetric unit, there are one unique Na atom, one unique Sr atom, one unique B atoms, and three unique O atoms (Table S1, ESI†). Each B atom is coordinated to three O atoms to form a planar BO_3 triangle (Fig. S4b, ESI†), with B–O bond lengths ranging from

1.366(7) to 1.396(7) Å and O–B–O bond angles ranging from 117.5(5) to 122.1(5)º (Table S2, ESI†). Each Na atom is bound to six O atoms to form a distorted NaO_6 octahedron (Fig. S4c, ESI†) with Na–O bond lengths between 2.286(4) and 2.608(4) Å. The 1D edge sharing chains are formed by every two NaO_6 octahedron sharing three O atoms (O(1), O(2), O(3)). $Sr(1)O_9$ polyhedra are interconnected by shared oxygen atoms form the 3D framework (Fig. S4d, ESI†) with Sr–O bond distances ranging from 2.596(4) to 2.848(4) Å. The isolated BO_3 groups connect the 1D edge sharing NaO_6 and 3D Sr–O framework to form the whole 3D network.

$Li_4CaB_2O_6$ crystallizes in space group *Pnnm* of the orthorhombic crystal system. In the asymmetric unit, there are two unique Li atom, one unique Ca atom, one unique B atoms, and three unique O atoms (Table S1, ESI†). The structure of $Li_4CaB_2O_6$ exhibits a three-dimensional (3D) network composed of LiO_n (n=4, 5), CaO_8 polyhedra, and isolated BO_3 groups (Fig. S5, ESI†). And every two $Li(1)O_5$ polyhedra are interconnected via sharing the O atoms into a 1D channels along the *c* axis. Then the 1D Li(2)–O channel and 1D $Li(1)O_3$ chain connect with each other to form a 3D framework. (Fig. S5c, ESI†). The 3D framework and 1D CaO_6 further connected by $B(1)O_3$ to generate a 3D network. In the framework, the Li-O bond lengths range from 1.931(3) to 2.227(5) Å with an average bond distance of 2.032 Å. And the B–O bond lengths range from 1.378(3) to 1.391(4) Å, bearing an average distance of 1.385 Å. The Ca atoms are coordinated to six O atoms, and the Ca atom stays in the center of the CaO_6 octahedron. The Ca–O bond lengths range from 2.333(2) to 2.435(3) Å bearing an average distance of 2.367 Å (Table S2, ESI†).

The bond valence sums of each atom are calculated[41,42] and are listed in Table S3, ESI†. The calculated total bond valences agree with the expected oxidation states.

Effect of Ions Substitution on Structural Transition

Interestingly, for $NaCaBO_3$ ($Na_3Ca_3B_3O_9$), as 2/3 Na^+ ions are substituted by Ca^{2+}, $NaCa_4B_3O_9$ is obtained. And after the substitution, the two structures have the same building block of isolated BO_3 group (Fig. 1). The CS crystal structure turn to the NCS space group ($NaCaBO_3$ adopts centric structure, while $NaCa_4B_3O_9$ adopts an acentric and polar structure) and both of them have many obvious differences in their structures.

First, the BO_3 units exhibit many differences in details. As described above, in $NaCaBO_3$, the arrangement of BO_3 are opposite and consequently the overall polar efficiency are cancelled. And in $NaCa_4B_3O_9$, $B(1)O_3$ and $B(2)O_3$ are arranged opposite, while $B(3)O_3$ are aligned in the *c* direction. The opposite arrangement about parts of BO_3 cancels parts of the SHG efficiency. So the compound has SHG efficiency about 1/2 KDP. Second, the different arrangement of the BO_3 building block should originate from different in the size of cations. In the structure of $NaCaBO_3$, the coordination environment of Ca^{2+} is 6/7-fold with the range of bond length about 2.2266(17)-2.6010(9) Å. And for Ca(1), the bond can divide into three groups, each of two has identical length about Ca(1)–O(4)=Ca(1)–O(4)#1= 2.2266(17) Å, Ca(1)–O(3)=Ca(1)–O(3)#1=2.3915(18) Å and Ca(1) –O(3)#2=Ca(1)–O(3)#3=2.3654(18) Å. In $NaCa_4B_3O_9$, the environment of Ca^{2+} is 8/9-fold with the range of bond length about 2.345(3)−2.8772(15) Å. That means, when a larger Ca^{2+} cation is introduced to replace the Na^+ cation, the original coordination configuration envronment of metal cation is destroyed, which leads to create an overall acentric distorted structure. This single connection reduces the possibility that the material crystallizes in the CS space group. That is what we hope in the design of NCS compound. Third, to better understand the effect of the Ca^{2+} substitution on structural transition, we further caculate the dipole moments in the BO_3 groups, and their contributions to the

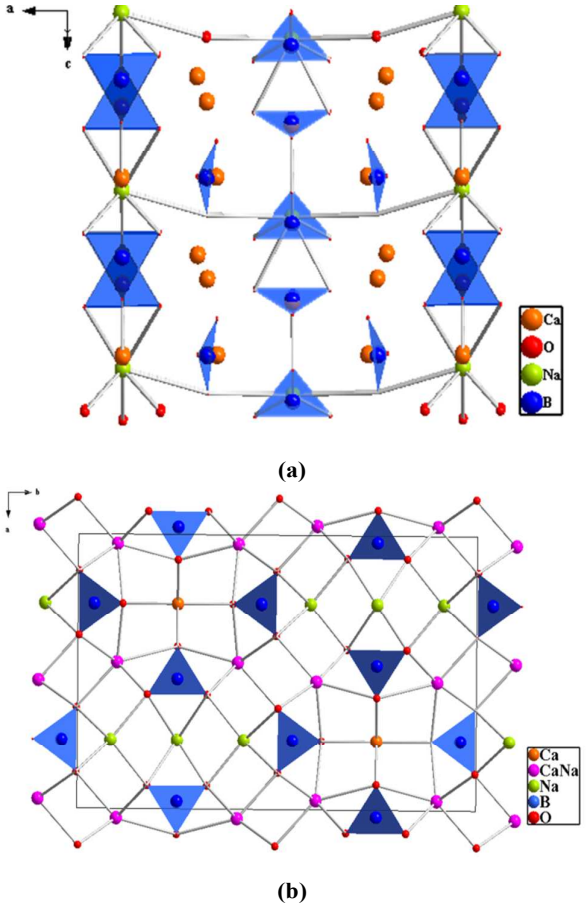

Fig. 2 The crystal structure of (a) $NaCa_4B_3O_9$ and (b) $NaCaBO_3$.

Table 2. Dipole moment caculations of $NaCa_4B_3O_9$ and $NaCaBO_3$.

compounds	species	x(*a*)	y(*b*)	z(*c*)	magnitude	
					deb ye	$\times10^{-4}$ esu·cm/Å^3
$NaCa_4B_3O_9$	$B(1)O_3$	0	-0.96	0.35	1.03	52.65
	$B(2)O_3$	0	0.80	-1.43	1.44	73.83
	$B(3)O_3$	0	0	0.09	0.09	4.85
	$Na(1)O_8$	0	3.48	2.63	4.36	223.65
	$Ca(1)O_8$	1.18	3.06	-0.28	3.29	168.85
	$Ca(2)O_9$	0	0	5.46	5.46	280.08
	$Ca(3)O_8$	0	-5.49	-2.21	5.92	303.55
	Unit Cell	0	0	17.30		
$NaCaBO_3$	$B(1)O_3$	0	0.31	1.40	1.44	0.02
	$B(2)O_3$	0.33	0	-0.41	0.53	0.01
	$Na(1)O_6$	0	0.597	2.18	6.35	0.09
	$Na(3)O_8$	0	0	-9.76	9.76	0.14
	$Ca(1)O_6$	0	0	2.04	2.01	0.03
	$Ca(2)O_7$	-1.98	-0.81	-1.02	2.37	0.03
	Unit Cell	0.00	0.00	0.00		

polarization in the unit cell with a simple bond–valence approach[40] (Table 2 and S4, ESI†). It is clear that the Ca–O group generates a net dipole moment along the *c* axis in the unit cell, while in $NaCaBO_3$ the dipole moments along all directions are cancelled. The results are consistent with the polarization observed from their crystal structures.

UV-VIS-NIR Diffuse-Reflectance Spectroscopy

The UV-VIS-NIR diffuse-reflectance spectra of $NaCa_4B_3O_9$, $NaCaBO_3$, $NaSrBO_3$ and $Li_4CaB_2O_6$ are shown in Fig. 3 and Fig. S6, ESI†. Absorption data are calculated from the Kubelka–Munk function. In a K–M vs E (eV) plot, extrapolating the linear part of the rising curve to zero provides the band gap about 4.30, 3.90, 3.20 and 3.50 eV for $NaCa_4B_3O_9$, $NaCaBO_3$, $NaSrBO_3$ and $Li_4CaB_2O_6$, respectively.[43,44]

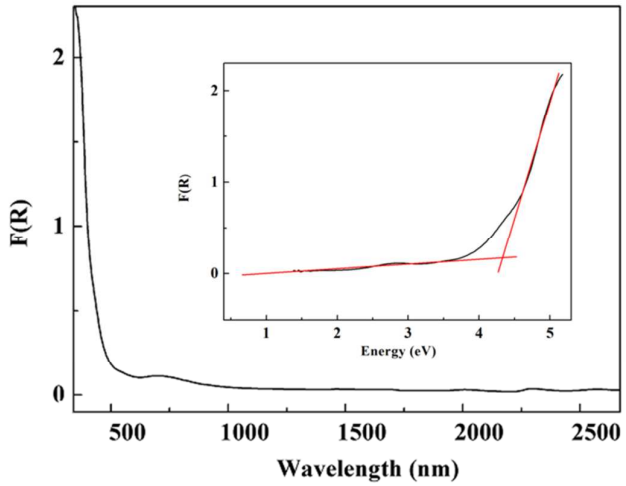

Fig. 3 The diffuse reflectance spectra for $NaCa_4B_3O_9$.

Band Structures and Density of States

The band structures of $NaCaBO_3$ and $NaCa_4B_3O_9$ are presented in Fig. S7, ESI†, and the lowest conduction band (LCB) energy and the highest valence band (HVB) energy of the first Brillouin zone are listed in Table S5, ESI†. The $NaCaBO_3$ and $NaCa_4B_3O_9$ compounds have direct band gaps of 3.78 and 4.17 eV, respectively. For $NaCa_4B_3O_9$, $KCa_4B_3O_9$ and $KSr_4B_3O_9$, they are isostructuralism. The band structures and density of states of $KCa_4B_3O_9$ and $KSr_4B_3O_9$ are also presented in Fig. S7, ESI†. Investigation of the band structure revealed that the fundamental absorption edges in $NaCa_4B_3O_9$, $KCa_4B_3O_9$ and $KSr_4B_3O_9$ correspond to direct gaps. The calculated band gaps (E_{calcd}=4.17 eV for $NaCa_4B_3O_9$, 4.37 eV for $KCa_4B_3O_9$ and 4.26 eV for $KSr_4B_3O_9$), just as expected from DFT method that the band gap is generally underestimated due to not sufficiently accuracy of exchange correlation energy were calculated.[45]

The total and partial densities of states (DOS and PDOS) are shown in Fig. 4. Th Na 2p orbitals are localized at about −22.5 eV. The VB spanning over −21.0 to −16.0 eV originates predominately from B 2s2p, O 2s and Ca 3p states, and a small portion of O 2s and Ca 3s states. The VBs ranging from −6.0 to −2.5 eV are mostly formed by B 2s2p states hybridized with correspond amounts of O 2s2p states. The VBs from −2.5 eV to the Fermi level (E_f) are mostly contributions of O 2p states with small amount of B 2s2p states. The B 2s2p, O 2s2p and Na 2s2p states mixing with Ca 3s3p state make up the conduction bands (CB) between 3.78 and 4.17 eV up to 10.0

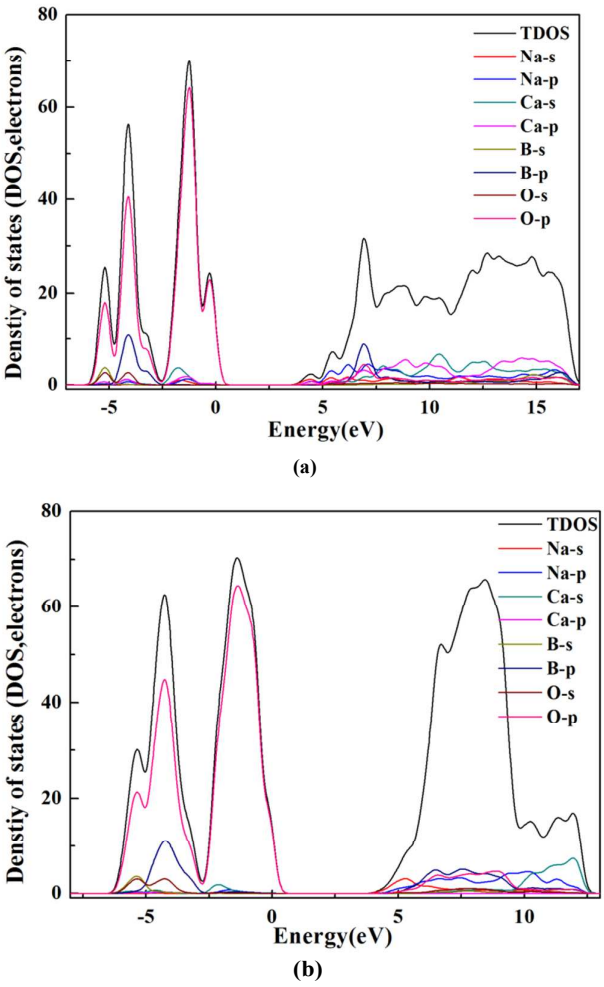

Fig. 4 The total and partial densities of states of (a) $NaCa_4B_3O_9$ and (b) $NaCaBO_3$.

eV. The CBs ranging from 10.0 to 13.0 eV mainly consist of Na 2s2p, B 2s2p and states with a small portion of Ca 3s.

It is interesting to note that, after 2/3 Na^+ ions are substituted by the Ca^{2+} ions, the bandgap of $NaCaBO_3$ is smaller than that of $NaCa_4B_3O_9$. In order to understand the origination of the difference, the authors carefully checked the electronic structures. As shown in Fig. 4, the components at the top of the valence band of these compounds are mainly O p states, while the states at the bottom of the conduction band are very different. The bottom of the conduction band of $NaCaBO_3$ are mainly Na sp states and Ca p states, while the states at the bottom of the conduction band of $NaCa_4B_3O_9$ are mainly Na sp states. As shown in Table S2 in ESI†, the bond length of Na-O bond of these two compounds are similar, while the bond length of Ca-O in $NaCaBO_3$ (2.2266(17)−2.6010(9) Å) is smaller than the Ca-O bond length in $NaCa_4B_3O_9$ (2.345(3)−2.8772(15) Å), indicating the relative large interaction of Ca and O can be found in $NaCaBO_3$, which make the site of Ca cations in $NaCaBO_3$ more close to the Fermi level, and then decrease the bandgap of $NaCaBO_3$.

The calculated projected density of states (PDOS) of $KCa_4B_3O_9$ and $KSr_4B_3O_9$ are shown in Fig. S8, ESI†. It is clearly shown that the O 2p states are dominated near Fermi level about -6.6 eV to 3.0

eV for $NaCa_4B_3O_9$, $KCa_4B_3O_9$ and $KSr_4B_3O_9$, this bands mostly originate from O 2p states with the mixings of B 2s2p and O 2s states, whereas there is an overlap between the 2p states of boron and oxygen atoms in the valence band region from -3.0 eV to Fermi level for $NaCa_4B_3O_9$, $KCa_4B_3O_9$ and $KSr_4B_3O_9$. It is worthy to note that there is no hybridizations occur below the Fermi level. From the atomic orbitals contribution, we can consider that the preferential contribution of cations orbitals to both VB and CB causes the width of band gap of $NaCa_4B_3O_9$, $KCa_4B_3O_9$ and $KSr_4B_3O_9$. In the case of $NaCa_4B_3O_9$, $KCa_4B_3O_9$ and $KSr_4B_3O_9$, the bottom of the conduction bands is mainly composed of 2p states of boron, oxygen, and orbitals of cations. For $NaCa_4B_3O_9$, $KCa_4B_3O_9$ and $KSr_4B_3O_9$, the conduction bands from CBM to 20.0 eV are mostly originate from Na 2s2p, K 3s3p, Ca 3s3p, Sr 4s4p and B 2s2p states with mixings of O 2s2p states.

Since the optical properties have relation with the electron transition from the top of valence band to the bottom of conduction band nearby Fermi level, one can deem that the BO_3 anionic groups have a dominant contribution to the SHG response for $NaCa_4B_3O_9$, $KCa_4B_3O_9$ and $KSr_4B_3O_9$, and the contribution of cations cannot be neglected especially for sodium, calcium, potassium or strontium whose orbitals have overlap with boron–oxygen atoms.

Optical Properties

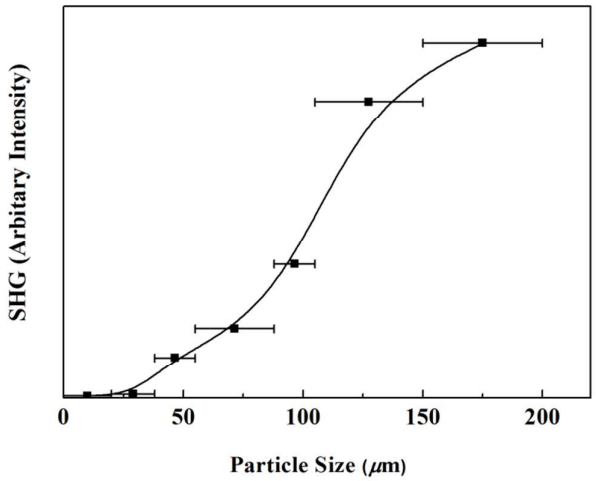

Fig. 5 Phase-matching curve, that is, particle size versus SHG intensity, data for $NaCa_4B_3O_9$. The solid curve drawn is to guide the eye and is not a fit to the data.

Fig. 5 gives the curve of SHG signal as a function of particle size made on ground $NaCa_4B_3O_9$ powder. Powder SHG measurements using 1064 nm radiation reveal that $NaCa_4B_3O_9$ is phase-matchable and has SHG efficiency comparable to that of 0.5 KDP (Fig. S9, ESI†). As the particle size of $NaCa_4B_3O_9$ becomes significantly larger than the coherence length of the material, the SHG intensity is independent of particle sizes. According to the anionic group theory of NLO activity in borates,[46] the BO_3 trigonal units are responsible for the large SHG effects. And also, the different orientations of the structure limit their total NLO contribution, so that the SHG coefficients are cancelled. As described in the crystal structure, the main SHG efficiency of the compound comes from the BO_3 triangles. As seen from Fig. 1, the SHG coefficients are cancelled because of the opposite arrangement about parts of BO_3. And then the resulting SHG effects are limited. Consequently, the overall SHG efficiency of $NaCa_4B_3O_9$ is merely about 0.5 KDP. It is consistent with the phase-matching behavior according to the rule proposed by Kurtz and Perry.

The SHG coefficients were also obtained on the basis of *ab initio* calculations. $NaCa_4B_3O_9$ belongs to *Ama*2 symmetry, consequently has three independent second-order tensors (χ_{31}, χ_{32} and χ_{33}) under the restriction of Kleinman symmetry which are twice the SHG coefficient of d_{31}, d_{32} and d_{33}. Thus, the calculated SHG coefficients for $NaCa_4B_3O_9$ are $d_{31} = 0.72$ pm/V, $d_{32} = 0.89$ pm/V and $d_{33} = 0.71$ pm/V, respectively.

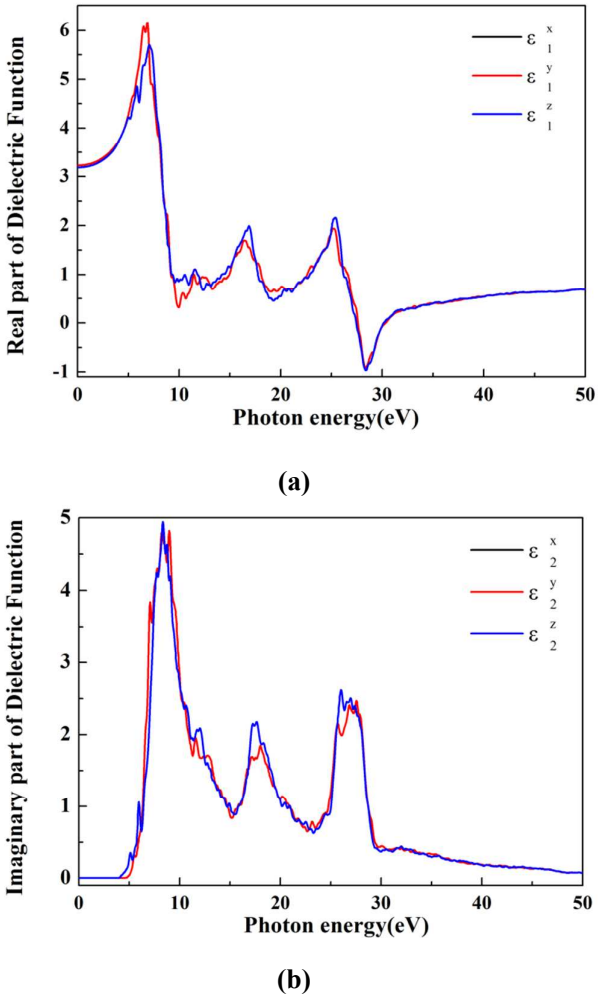

Fig. 6 The calculated parts real (a) and imaginary parts (b) of frequency-dependent dielectric function along three principal dielectric axes of $NaCa_4B_3O_9$.

Since $NaCa_4B_3O_9$ crystallizes in the polar space group, it is worthy to analyse the structure–property relationship of $NaCa_4B_3O_9$. As described in the crystal structure, the main SHG efficiency of the compound comes from the BO_3 triangles. The direction and magnitude of the isolated planar BO_3 triangles have been quantified by determining the local dipole moments. This method uses a bond-valence approach to calculate the direction and magnitude of the dipole moment.[40] The polarization of $NaCa_4B_3O_9$ in the unit cell and

the contributions from the BO_3 groups have been shown in Table S4, ESI†. It is clear that although the polarizations of all the BO_3 groups along the *a*- and *b*-axis are cancelled, and the vector sum of them is reflected along the *c* axis (Fig. 1).

The linear optical response properties of the compounds were examined through calculating the complex dielectric function $\varepsilon(\omega) = \varepsilon1(\omega) + i\varepsilon2(\omega)$.[47] The energy dependence of the real part ε_1 and imaginary part ε_2 are displayed in Fig. 6. The imaginary part ε_2 can be used to describe the real transitions between the occupied and unoccupied electronic states. The imaginary and real parts of the frequency-dependent dielectric functions show obvious anisotropy along different dielectric axis directions. The averaged imaginary parts reveal the strongest adsorption peaks of $NaCa_4B_3O_9$ at 4.17 eV (Fig. 6b), which can be mainly assigned to the electronic interband transitions from the O 2p and B 2p, Na 2p/Ca 3p. The dispersion curves of refractive indices calculated according to the formula $n^2(\omega) = \varepsilon(\omega)$ display strong anisotropy: $n^x \approx n^y > n^z$ for $NaCa_4B_3O_9$ and the curve of birefringence (Δn) versus wavelength is shown in Fig. 7 and Fig. S10, ESI† show that $NaCa_4B_3O_9$, $KCa_4B_3O_9$ and $KSr_4B_3O_9$ possesse moderate birefringence and the birefringence Δn are equal to 0.05, 0.067 and 0.028 at 1064 nm ($\Delta n = n^z - n^x$).

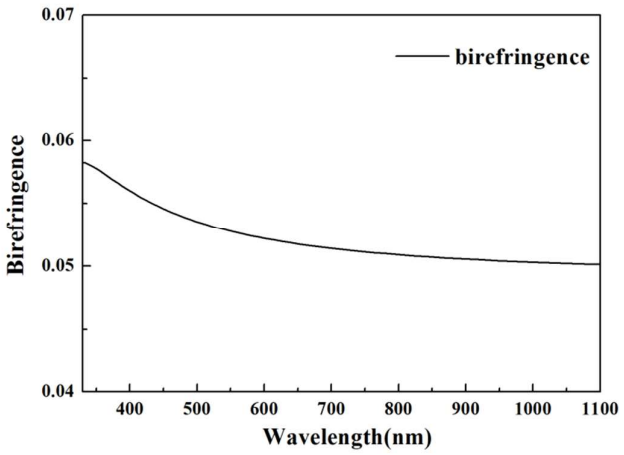

Fig. 7 The wavelength dependence of refractive indices where the direction of the electric field parallels to *a*-axis (n_x) or *c*-axis (n_z) of $NaCa_4B_3O_9$.

4. Conclusions

In summary, pure sample and single crystals of $NaCa_4B_3O_9$, $NaCaBO_3$, $NaSrBO_3$ and $Li_4CaB_2O_6$ have been prepared and structurally characterized by single crystal X-ray diffraction. There are some interesting connections in the crystal structure. From CS compound $NaCaBO_3$ to NCS compound $NaCa_4B_3O_9$, we discuss the influence of ionic substitution on the structure and properties of compounds. Detailed structural analyses show that the larger metal Ca^{2+} cations destroy the original coordination configuration envronment and leads to an overall acentric distorted structure. This single connection reduces the possibility that the material crystallizes in the CS space group. It is very helpful in the design of NCS compounds. Studies of their optical properties as well as band structure calculations based on first principles have been also performed on the title compounds ($NaCa_4B_3O_9$) and ranging to the compounds with similar structure ($KCa_4B_3O_9$ and $KSr_4B_3O_9$). Base on the electronic structures of $NaCa_4B_3O_9$, $KCa_4B_3O_9$ and $KSr_4B_3O_9$ crystals, in particular at the bottom of conduction band (CB) and the top of valence band (VB), since they are known to play a primary role in SHG. The theoretical results not only explain that the BO_3 anionic groups have a dominant contribution to the SHG response for $NaCa_4B_3O_9$, $KCa_4B_3O_9$ and $KSr_4B_3O_9$, but also the effect of cations cannot be neglected especially for sodium, calcium, potassium or strontium whose orbitals have overlap with boron–oxygen atoms. $NaCa_4B_3O_9$, $KCa_4B_3O_9$ and $KSr_4B_3O_9$ possesse moderate birefringence and the birefringence Δn are equal to 0.05, 0.067 and 0.028 at 1064 nm

Acknowledgements

This work is supported by 973 Program of China (Grant Nos. 2014CB648400), the National Natural Science Foundation of China (Grant Nos. U1303193), the National Science Foundation of Xinjiang Uygur Autonomous Region (No. 2013200B35)..

Notes and references

(1) (a) H. Y. Chang, S. H. Kim, P. S. Halasyamani and K. M. Ok, *J. Am. Chem. Soc.* 2009, **131**, 2426-2427. (b) P. S. Halasyamani and K. R. Poeppelmeier, *Chem. Mater.* 1998, **10**, 2753-2769. (c) A. J. Norquist, K. R. Heier, P. S. Halasyamani, C. L. Stern and K. R. Poeppelmeier, *Inorg. Chem.* 2001, **40**, 2015-2019. (d) S. B. Lang, *Phys. Today* 2005, **58**, 31-36.

(2) R. K. Li and Y.Yu, *Inorg. Chem.* 2006, **45**, 6840-6843.

(3) (a) C. F. Sun, C. L. Hu, X. Xu, J. B. Ling, T. Hu, F. Kong, X. F. Long and J. G. Mao, *J. Am. Chem. Soc.* 2009, **131**, 9486-9487. (b) J. H. Zhang, F. Kong and J. G. Mao, *Inorg. Chem.* 2011, **50**, 3037-3043.

(4) (a) S. C. Wang and N. Ye, *J. Am. Chem. Soc.* 2013, **133**, 11458-11461. (b) S. C. Wang, N. Ye, W. Li and D. Zhao, *J. Am. Chem. Soc.* 2010, **132**, 8779-8786.

(5) (a) H. W. Huang, L. J. Liu, S. F. Jin, W. J. Yao, Y. H. Zhang, and C. T. Chen, *J. Am. Chem. Soc.* 2013, **49**, 18319-18322. (b) H. W. Huang, J. Y. Yao, Z. S. Lin, X. Y. Wang, R. He, W. J. Yao, N. X. Zhai and C. T. Chen, *Chem. Mater.* 2011, **23**, 5457-5463.(c) H. W. Huang, J. Y. Yao, Z. S. Lin, X. Wang, R. He, W. Yao, N. Zhai and C.T. Chen, *Angew. Chem. Int. Ed.* 2011, **50**, 9141-9144.

(6) (a) H. Y. Chang, S. H. Kim, K. M. Ok and P. S. Halas H. W. Huang, J. Y. Yao, Z. S. Lin, X. Wang, R. He, W. Yao, N. Zhai and C.T. Chen, *Angew. Chem. Int. Ed.* 2011, **50**, 9141-9144.yamani, *J. Am. Chem. Soc.* 2009, **131**, 6865-6873.(b) E. O. Chi, A. Gandini, K. M. Ok, L. Zhang and P. S. Halasyamani, *Chem. Mater.* 2004, **16**, 3616-3622. (c) K. M. Ok, J. Baek, P. S. Halasyamani and D. Hare, *Inorg. Chem.* 2006, **45**, 10207-10214. (d) S. W. Bae, C. Y. Kim, D. W. Lee and K. M. Ok, *Inorg. Chem.* 2014, **53**, 11328-11334.

(7) (a) H. W. Yu, S. L. Pan, H. P. Wu, Z. H. Yang, L. Y. Dong, X. Su, B. B. Zhang and H. Y. Li, *Cryst. Growth Des.* 2013, **13**, 3514-3521. (b) S. J. Han, Y. Wang, S. L. Pan, X. Y. Dong, H. P. Wu, J. Han, Y. Yang, H. W. Yu, and C. Y. Bai, *Cryst. Growth Des.* 2014, **14**, 1794-1801.

(8) (a) Y. Z. Huang, L. M. Wu, X. T. Wu, L. H. Li, L. Chen and Y. F. Zhang, *J. Am. Chem. Soc*. 2010, **132**, 12788-12789.

(9) (a) C. Rong, Z. W. Yu, Q. Wang, S. T. Zheng, C. Y. Pan, F. Deng and G. Y. Yang, *Inorg. Chem.* 2009, **48**, 3650-3659. (b) H. X. Zhang, J. Zhang, S. T. Zheng and G. Y. Yang, *Cryst. Growth Des.* 2005, **5**, 157-161.

(10) (a) X. A. Chen, M. Li, X. A. Chang, H. G. Zang and W. Q. Xiao, *J. Solid State Chem.* 2007, **180**, 1658-1663. (b) X. A. Chen, H. Yin, X. A. Chang, H. G. Zang and W. Q. Xiao, *J. Solid State* 2010, **183**, 2910-2916.

(11) (a) H. P. Wu, H. W. Yu, S. L. Pan, A. Q. Jiao, J. Han, K. Wu and S. J. Han, *Dalton Trans.* 2014, **43**, 4886-4891.(b) Z. Wang, M. Zhang, S. L. Pan, Y. Wang and H. Zhang, *Dalton Trans.* 2014, **43**, 2828-2834. (c) H. P. Wu, H. W. Yu, Z. H. Yang, X. L. Hou, X. Su, S. L. Pan, K. R.

Poeppelmeier and J. M. Rondinelli, *J. Am. Chem. Soc.* 2013, **135**, 4215-4218. (d) X. Y. Dong, Y. J. Shi, Z. H. Yang, B. B. Zhang, Z. H. Chen, Y. Yang, Z. J. Huang, S. L. Pan and Z. X. Zhou, *Chem.-Eur. J.* 2013, **19**, 7338-7341. (e) H. W. Yu, H. P. Wu, S. L. Pan, Y. Wang, X. Su and Z. H. Yang, *Inorg. Chem.* 2013, **52**, 5359-5365. (f) H. W. Yu, H. P. Wu, S. L. Pan, Z. H. Yang, X. Su and F. F. Zhang, *J. Mater. Chem.* 2012, **22**, 9665-9670.

(12) (a) C. T. Chen, B. C. Wu, A. D. Jiang and G. M. You, *Sci. Sin. B* 1985, **28**, 235-241. (b) C. T. Chen and G. Liu, *Annu. Rev. Mater. Sci.* 1986, **16**, 203-243. (c) C. T. Chen, Y. C. Wu and R. K. Li, *Int. Rev. Phys. Chem.* 1989, **8**, 65-91. (d) C. T. Chen, Z. S. Lin and Z. Wang, *Appl. Phys. B* 2005, **80**, 1-25.

(13) (a) C. T. Chen, Y. C. Wu, A. D. Jiang, G. M. You, R. K. Li and S. J. Lin, *J. Opt. Soc. Am. B* 1989, **6**, 616-621. (b) E. Bétourné and M. Touboul, *J. Alloys Compd.* 1997, **255**, 91-97.

(14) (a) Y. C. Wu, T. Sasaki, S. Nakai, A. Yokotani, H. Tang and C. T. Chen, *Appl. Phys. Lett.* 1993, **62**, 2614-2615. (b) M. Touboul, N. Penin and G. Nowogrocki, *J. Solid State Chem.* 1999, **143**, 260-265.

(15) (a) Y. Mori, I. Kuroda, S. Nakajima, T. Sasaki and S. Nakai, *Appl. Phys. Lett.* 1995, **67**, 1818-1820. (b) J. M. Tu and D. A. Keszler, *Mater. Res. Bull.* 1995, **30**, 209-215.

(16) (a) C. T. Chen, J. H. Lu, T. Togashi, T. Suganuma, T. Sekikawa, S. Watanabe, Z. Y. Xu and J. Y. Wang, *Opt. Lett.* 2002, **27**, 637-639. (b) B. C. Wu, D. Y. Tang, N. Ye and C. T. Chen, *Opt. Mater.* 1996, **5**, 105-109.

(17) T. Sasaki, Y. Mori, M. Yoshiura, Y. K. Yap and T. Kamimura, *Mater. Sci. Eng. R: Rep.* 2000, **30**, 1-54.

(18) C. D. McMillen, J. T. Stritzinger and J. W. Kolis, *Inorg. Chem.* 2012, **51**, 3953-3955.

(19) H. Huppertz and B. von der Eltz, *J. Am. Chem. Soc.* 2002, **124**, 9367-9377.

(20) M. J. Xia and R. K. Li, *J. Solid. State .Chem.* 2013, **197**, 366-369.

(21) N. I. Leonyuk and L. I. Leonyuk, Prog. *Cryst. Growth Charact.* 1995, **31**, 179-278.

(22) (a) D. F. Xue, K. Betzler, H. Hesse and D. Lammers, *Solid State Commun.* 2010, **114**, 21-25. (b) G. H. Yuan and D. F. Xue, *Acta Crystallogr. B* 2007, **63**, 353-362. (c) D. Q. Yu and D. F. Xue, *Acta Crystallogr. B* 2006, **62**, 702-709. (d) D. F. Xue and S. Y. Zhang, Chem. *Phys. Lett.* 1999, **301**, 449-452. (e) D. F. Xue and H. Ratajczak, *J. Mol. Struct.* (Theochem), 2005, **716**, 207-210.

(23) (a) Z. S. Lin, Z. Z. Wang, C. T. Chen and M. H. Lee, *J. Appl. Phys.* 2001, **90**, 5585-5590.

(24) (a) J. G. M. Jesudurai, K. Prabha, P. D. Christy, J. Madhavan and P. Sagayaraj, *Spectrochim. Acta A* 2008, **71**, 1371-1378. (a) R. W. Whatmore, N. M. Shorrocks, C. O'Hara, F. W. Ainger and I. M. Young, *Electron. Lett.* 1981, **17**, 11-12. (b) I. N. Ogorodnikov, V. Y. Yakovlev and L. I. Isaenko, *Radiat. Meas.* 2004, **38**, 659-662.

(25) (a) L. Wu, X. L. Chen, Y. P. Xu and Y. P. Sun, *Inorg. Chem.* 2006, **45**, 3042-3047. (b) L. Wu, X. L. Chen, X. Z. Li, L. Dai, Y. P. Xu and M. Zhao, *Acta Crystallogr. Sect. C: Cryst. Struct. Commun.* 2005, **C61**, i32-i34. (c) L. Wu, X. L. Chen, H. Li, M. He, Y. P. Xu and X. Z. Li, *Inorg. Chem.* 2005, **44**, 6409-6414. (d) L. Wu, X. L. Chen, Y. Zhang, Y. F. Kong, J. J. Xua and Y. P. Xu, *J. Solid. State .Chem.* 2006, **179**, 1219-1224. (e) L. Wu, X. L. Chen, H. Li, M. He, L. Dai, X.Z. Li and Y.P. Xu, *J. Solid State Chem.* 2004, **177**, 1111-1116. (f) L. Wu, C. Wang, X. L. Chen, X. Z. Li, Y. P. Xu and Y. G. Cao, *J. Solid State Chem.* 2004, **177**, 1847-1851.

(26) (a) J. P. Perdew, K. Burke and M. Ernzerhof, *Phys. Rev. Lett.* 1996, **77**, 3865-3868. (b) J. S. Lin, A. Qteish, M. C. Payne and V. Heine, *Phys. Rev. B.* 1993, **47**, 4174-4180. (c) A. M. Rappe, K. M. Rabe, E. Kaxiras and J. D. Joannopoulos, *Phys. Rev. B* 1990, **41**, 1227-1230.

(27) SAINT-Plus, version 6.02A; Bruker Analytical X-ray Instruments, Inc.: Madison, WI, 2000.

(28) G. M. Sheldrick, SHELXTL, Version 6.14; Bruker Analytical X-ray Instruments, Inc.: Madison, WI, 2003.

(29) G. M. Sheldrick, SHELXS-97, Program for X-ray Crystal Structure Solution; University of Göttingen: Göttingen, Germany, 1997

(30) A. L. Spek, *J. Appl. Crystallogr.* 2003, **36**, 7-13.

(31) (a) S. Q. Kurtz and T. T. Perry, *J. Appl. Phys.* 1968, **39**, 3798-3813. (b) J. P. Dougherty and S. K. Kurtz, *J. Appl. Crystallogr.* 1976, **9**, 145-158.

(32) (a) X. Y. Fan, S. L. Pan, X. L. Hou, X. L. Tian, J. Han, J. Haag and K. R Poeppelmeier, *Cryst. Growth Des.* 2010, **10**, 252-256. (b) F. Li, S. L. Pan, X. L. Hou and J. Yao, *Cryst. Growth Des.* 2009, **9**, 4091-4095. (c) Y. J. Wang, S. L. Pan, X. L. Hou, Z. X. Zhou, G. Liu, J. D. Wang and D. Z. Jia, *Inorg. Chem.* 2009, **48**, 7800-7804.

(33) S. J. Clark, M. D. Segall, Pickard, C. J. P. J. Hasnip, M. J. Probert, K. Rrfson and M. C. Payne, *Z. Kristallogr.* 2005, **220**, 567-570.

(34) H. J. Monkhorst and J. D. Pack, *Phys. Rev. B* 1976, **13**, 5188-5192.

(35) E. D. Palik, *Handbook of Optical Constants of Solids*. Orlando: Academic Press: New York, 1985.

(36) F. Wooten, Optical Properties of Solid (Academic, New York, 1972

(37) C. Aversa and J. E. Sipe, *Phys. Rev. B* 1995, **52**, 14636−14645.

(38) J. Lin, M. H. Lee, Z. P. Liu, C. Chen and C. J. Pickard, *Phys. Rev. B* 1999, **60**, 13380−13389.

(39) (a) B. B. Zhang, M. H. Lee, Z. H Yang, Q. Jing, S. L. Pan, M. Zhang, H. P. Wu, X. Su, C. S. Li, *Appl. Phys. Lett.* 2015, 106, 031906-031911. (b) F. Y. Zhang, F. F. Zhang, Q. Jing, S. L. Pan, Z. H. Yang, D. Z. Jia, *Phys. Chem. Chem. Phys.* 2015, **17**, 10489-10496. (c) X. Su, Z. H. Yang, M. H. Le, S. L. Pan, Y. Wang, X. Y. Fan, Z. J. Huang, B. B. Zhang, *Phys. Chem. Chem. Phys.* 2015, **17**, 5338-5344. (d) C. Lei, Z. H. Yang, M. H. Le, Q. Jing, Z. H. Chen, X. C. Huang, Y. Wang, S. L. Pan, M. R. S. A. Janjua, *Phys. Chem. Chem. Phys.* 2014, **16**, 20089-20096. (e) X. Su, Y. Wang, Z. H. Yang, X. C. Huang, S. L. Pan, F. Li, M. H. Lee, *J. Phys. Chem. C* 2013, **117**, 14149−14157. (f) B. B. Zhang, Z. H. Yang, Y. Yang, M. H. Lee, S. L. Pan, Q. Jing, X. Su, *J. Mater. Chem. C* 2014, **2**, 4133−4141.

(40) (a) K. M. Ok and P. S. Halasymani, *Inorg. Chem.* 2005, **44**, 3919-3925. (b) H. W. Yu, S. L. Pan, H. P. Wu, W. W. Zhao, F. F. Zhang, H. Y. Li and Z. H. Yang, *J. Mater. Chem.* 2012, **22**, 2105-2110. (c) P. A. Maggard, T. S. Nault, C. L. Stern and K. R. Poeppelmeier, *J. Solid State Chem.* 2003, **175**, 27-33.

(41) (a) I. D. Brown and D. Altermatt, *Acta Crystallogr. B* 1985, **41**, 244-247. (b) N. E. Brese and M. O'Keeffe, *Acta Crystallogr. B* 1991, **47**, 192-197.

(42) F. F. Zhang, K. Y. Li, H. Ratajczak and D. F. Xue, *J. Mol. Struct.* 2010, **976**, 69-72.

(43) J. P. Perdew and M. Levy, *Phys. Rev. Lett.* 1983, **50**, 1884.

(44) (a) L. J. Liu, C. L. Liu, X. Y. Wang, Z. G. Hu, R.K. Li and C. T. Chen, *Solid State Sci.* 2009, **11**, 841-844. (b) L. J. Liu and C. T. Chen, *J. Cryst. Growth*, 2006, **292**, 472-475.

(45) R. W. Godby, M. Schluter, L. J. Sham, *Phys. Rev. B* 1987, **36**, 6497-6550.

(46) (a) C. T. Chen, Y. C. Wu and R. C. Li, *J. Cryst. Growth* 1990, **99**, 790-798. (b) X. Sun, C. Q. Zhang and X. T. Tao, *Chem. Mater.* 2011, **23**, 3752-3761.

(47) F. Wooten, Optical Properties of Solid (Academic, New York, 1972).